Instabilities of breathers in a finite NLS lattice

Panayotis Panayotaros *

Depto. Matemáticas y Mecánica, I.I.M.A.S.-U.N.A.M., Apdo. Postal 20–726, 01000 México D.F., Mexico

ABSTRACT

We study some aspects of the dynamics of unstable breathers in a three-site discrete cubic NLS chain with Dirichlet boundary conditions. We view breathers as fixed points of the energy in the reduced phase space obtained by eliminating directions related to the global phase symmetry of the system. We use a combination of numerical calculations and Morse-theoretical arguments to see that there are two breathers that correspond to critical energies where the energy hypersurface changes its connectivity. These breathers are elliptic–hyperbolic fixed points of the reduced four-dimensional system. We compute the periodic orbits in their center manifolds (Lyapunov orbits) and see evidence for homoclinic intersections of their stable and unstable manifolds. We also examine the possibility of heteroclinic connections between Lyapunov orbits, these however appear not to exist for the energies near the energy where the energy hypersurface becomes connected.

© 2012 Elsevier B.V. All rights reserved.

1. Introduction

In this paper we study instabilities of some breather solutions in a discrete nonlinear Schrödinger (NLS) equation in a finite lattice. The discrete NLS equation models several physical systems in areas such as nonlinear optics [1,2], Bose–Einstein condensates [3], and molecular chains [4], and is one of the simplest models used to study the interplay between spatial inhomogeneity and nonlinearity, as well as basic questions on the dynamics of nonlinear chains; see e.g. [5].

Breather solutions are usually studied in the context of localization in nonlinear lattice systems. The phenomenon of localization due to nonlinearity is very robust and the precise definition of a breather solution may depend on the model. In the case of NLS type equations in finite lattices, and other Hamiltonian systems with a global S^1 symmetry, breathers are usually defined as relative equilibria of the S^1 symmetry and correspond to fixed points of the reduced system obtained by symplectic reduction of the S^1 action; see e.g. [6, Chapter 4.3]. Breathers are thus the simplest nontrivial solutions of such systems and are also interesting for studies of their global dynamics. In this work we focus on the one dimensional discrete cubic NLS with Dirichlet boundary conditions where we have a better knowledge of the breather solutions as the parameters of the system are varied; see [7–9]. We also use a coordinate system in which the equations

on the reduced phase space have the standard canonical form of Hamilton's equations.

From earlier analytical and numerical results on the stability of breathers, see [10], we know that the reduced phase space has many elliptic–hyperbolic fixed points, moreover the number of elliptic and hyperbolic directions can vary with the parameters of the system. We want to examine the possibility of homoclinic and heteroclinic intersections of stable and unstable manifolds of invariant sets in the vicinity of the fixed points, and relate this information to energy localization and transport, e.g. the existence of unstable yet recurrent spatially localized solutions, trajectories that connect one spatially localized solution to another, etc. The general problem is outside the scope of the present work, and here we examine the simplest nontrivial case of a lattice with three sites where the reduced phase space is four dimensional (see e.g. [4,9] for applications of such systems). In this system we have a pair of elliptic–hyperbolic fixed points that correspond to concentration of the energy in two consecutive sites and we study numerically the stable and unstable manifolds of the periodic orbits (Lyapunov orbits) in the vicinity of the breather relative equilibria. Our work is also inspired by the numerical study of a similar problem arising in the restricted three-body problem by Canalias et al. [11]. In the present case we show evidence that the two fixed points we consider also correspond to the critical points of the energy for which we pass from a non-connected to a connected energy hypersurface. Thus we are also interested in relating stable and unstable manifolds to trajectories that connect different subregions of the energy hypersurface after the energy hypersurface becomes connected.

* Tel.: +52 55 5622 3600; fax: +52 55 5622 3564.
E-mail address: panos@mym.iimas.unam.mx.

The existence of periodic orbits around the two fixed points follows from standard results and here we compute these orbits numerically. Integrating from suitable initial conditions in the vicinity of the periodic orbits we obtain approximations of their stable and unstable manifolds and show evidence for the existence of orbits that are homoclinic to the periodic orbits. The computed pieces of the stable and unstable manifolds of the fixed points and the periodic orbits imply that energy can be localized in unstable but recurrent ways in two sites. We also examine the respective stable and unstable manifolds of the two fixed points and see that they remain far apart. As we move further below the critical energy by considering periodic orbits that are farther from each of the fixed points we see that the distance between (the computed pieces of) their respective stable and unstable manifolds diminishes but does not vanish. Thus we do not see any evidence for heteroclinic intersections for energies near the critical energy.

The paper is organized as follows. In Section 2 we describe the reduced phase space for the discrete NLS with Dirichlet boundary conditions, and more general systems. We discuss known breather solutions for $N = 3$ and use this information to examine the connectivity of the energy hypersurface in the reduced phase space. In Section 3 we describe the numerical construction of Lyapunov orbits near elliptic–hyperbolic breathers and present numerical results on possible homoclinic and heteroclinic intersections. In the Appendix we also discuss relative stability results for breathers, comparing the moving reference frame and reduced phase space approaches.

2. Breathers of the finite NLS model

We consider the discrete NLS equation on a finite lattice

$$\dot{u}_n = i\delta(\Delta u)_n - 2i|u_n|^2 u_n, \quad n \in \iota_N = \{1, \ldots, N\}, \tag{2.1}$$

where Δ is defined by $(\Delta u)_n = u_{n+1} + u_{n-1} - 2u_n, n = 2, \ldots, N-1$, and $(\Delta u)_1 = u_2 - 2u_1$, $(\Delta u)_N = u_{N-1} - 2u_N$. The site coupling constant δ is real and we also note that the definition of Δu at the endpoints here is analogous to imposing *Dirichlet* boundary conditions.

System (2.1) can be also written in the complex form of Hamilton's equations

$$\dot{u}_n = -i\frac{\partial H}{\partial u_n^*}, \quad n \in \iota_N, \text{ with} \tag{2.2}$$

$$H = \delta\left(\sum_{n=1}^{N-1}|u_{n+1} - u_n|^2 + |u_1|^2 + |u_N|^2\right) + \sum_{n=1}^{N}|u_n|^4. \tag{2.3}$$

Alternatively, we can write (2.2) as $\dot{z} = J\nabla\tilde{H}$, with $z = [q_1, \ldots, q_n, p_1, \ldots, p_n]^T \in \mathbf{R}^{2N}$, $\tilde{H} = \frac{1}{2}H$, $u_n = q_n + ip_n$, $n \in \iota_N$, and J the standard symplectic matrix in $\mathbf{R}^{2N}$. We denote the corresponding Poisson bracket by $[\,,\,]$. H is invariant under the S^1 action of global phase change $(e^{i\theta}, u) \mapsto e^{i\theta}u$, with $\theta \in \mathbf{R}$ (independent of n). The orbits of this action are obtained by integrating the Hamiltonian flow of $P = \sum_{n\in\iota_N}|u_n|^2$. Clearly, P is a conserved quantity and Poisson commutes with H.

For $N = 2$ system (2.1) is integrable, since the conserved quantities H, P are easily seen to satisfy the axioms of integrability. Larger lattices on the other hand are not known to be integrable. To study the $N = 3$ case we use a reduced phase space defined in [7] for arbitrary $N \geq 2$. In particular, introduce (polar) coordinates J_n, ϕ_n by $u_n = \sqrt{J_n}e^{i\phi_n}$, $n \in \iota_N$, and define θ_n, I_n by

$$\theta_n = \phi_{n+1} - \phi_n, \quad n = 1, \ldots, N-1, \qquad \theta_N = \sum_{n=1}^{N}\phi_n \tag{2.4}$$

$$J_1 = I_1 + I_N, \qquad J_n = I_n - I_{n-1} + I_N, \quad n = 2, \ldots, N-1,$$
$$J_N = I_N - I_{N-1}. \tag{2.5}$$

Then (2.1) becomes

$$\dot{I}_n = \frac{\partial h}{\partial \theta_n}, \qquad \dot{\theta}_n = -\frac{\partial h}{\partial I_n}, \quad n \in \iota_N, \text{ with } h = H. \tag{2.6}$$

System (2.6) is defined for $(I, \theta) \in \mathbf{S}^N \times \mathbf{T}^N$, where $\mathbf{S}^N$ is the set of $I = [I_1, \ldots, I_N] \in \mathbf{R}^N$ such that $J_1 > 0, \ldots, J_N > 0$ in (2.5), and $\mathbf{T}^N$ is the N-torus. We denote the above change of variables as $u = f(I, \theta)$.

The Poisson bracket of P and H is seen to be proportional to the directional derivative of H along θ_N, and since P and H Poisson commute we have that h is independent of θ_N. Therefore I_N is conserved. In fact, $I_N = N^{-1}P$ by (2.5) and we recover the conservation of P. Let $h_c = h|_{I_N=c}$. Since h is C^1 in $\mathbf{S}^N \times \mathbf{T}^N$, we also have $(\partial_{\theta_i}h)|_{I_N=c} = \partial_{\theta_i}h_c$, $(\partial_{I_j}h)|_{I_N=c} = \partial_{I_j}h_c$, $\forall i, j \in \iota_{N-1}$. Then (2.6) implies that for every $c > 0$, the variables $\bar{I} = [I_1, \ldots, I_{N-1}]$, $\bar{\theta} = [\theta_1, \ldots, \theta_{N-1}]$ evolve according to the *reduced system*

$$\dot{I}_n = \frac{\partial h_c}{\partial \theta_n}, \qquad \dot{\theta}_n = -\frac{\partial h_c}{\partial I_n}, \quad n \in \iota_{N-1}. \tag{2.7}$$

System (2.7) is defined for $(\bar{I}, \bar{\theta}) \in \mathbf{S}_c^{N-1} \times \mathbf{T}^{N-1}$ where $\mathbf{S}_c^{N-1}$ is the set of $[I_1, \ldots, I_{N-1}] \in \mathbf{R}^{N-1}$ satisfying $J_1 > 0, \ldots, J_N > 0$ in (2.5) with $I_N = c$.

The above construction falls within the general framework of symplectic reduction; see [6, Chapter 4.3]. We see that $\mathcal{M} = \mathbf{S}_c^{N-1} \times \mathbf{T}^{N-1}$ can be identified with an open subset of the reduced phase space $\overline{\mathcal{M}} = P^{-1}(Nc)/S^1$, $c > 0$, which is here the complex projective space $\mathbf{CP}^{N-1}$. Alternatively, the reduced action-angle variables $\bar{I} \in \mathbf{S}_c^{N-1}$, $\bar{\theta} \in (0, 2\pi)^{N-1}$ can be viewed as a particular system of coordinates on $\mathbf{CP}^{N-1}$ in which the reduced system takes the standard form of Hamilton's equations (2.7). These observations follow from the definition of $\mathbf{CP}^{N-1}$ as the set of points of the unit sphere S^{2N-1} in $\mathbf{C}^N$ modulo orbit equivalence under the "diagonal" S^1 action $(e^{i\theta}, z) \mapsto e^{i\theta}z$, $z \in \mathbf{C}^N$, $\theta \in \mathbf{R}$, i.e. the diagonal action is the global phase change defined earlier. $\mathcal{M}$ is then $\mathbf{CP}^{N-1}$ minus the points obtained by starting from the $z \in S^{2N-1} \subset \mathbf{C}^N$ that have at least one vanishing component. Neighborhoods of points of $\overline{\mathcal{M}} \setminus \mathcal{M}$ can be covered by other coordinate systems; see e.g. [12, p. 26].

Remark 2.1. The reduction using the variables $\bar{I}$, $\bar{\theta}$ is also applicable to other discrete NLS equations of the form (2.2) on ι_N, provided that their Hamiltonian Poisson commutes with P. Examples include the analogue of (2.1) with periodic boundary conditions, higher dimensional analogues, as well as equations with more general nonlinearities and couplings between the sites.

In the case $N = 3$, (2.4), (2.5), and $I_3 = c$ lead to the reduced action-angle variables

$$I_1 = J_1 - c, \qquad I_2 = \frac{1}{2}(J_1 + J_2 - J_3 - c),$$
$$\theta_1 = \phi_2 - \phi_1,$$
$$\theta_2 = \phi_3 - \phi_2. \tag{2.8}$$

$[I_1, I_2, \theta_1, \theta_2] \in \mathbf{S}_c^2 \times \mathbf{T}^2$, where $\mathbf{S}_c^2$ is the interior of the triangle defined by $(-c, c)$, $(-c, -2c)$, $(2c, c)$. Each side of the triangle

corresponds to the vanishing of one of the J_k, $k = 1, 2, 3$. The reduced equation is (2.7), $N = 3$, with

$$h_c = [(I_1 + c)^2 + (I_2 - I_1 + c)^2 + (c - I_2)^2]$$
$$- 2\delta \left[\sqrt{(I_1 + c)(I_2 - I_1 + c)} \cos \theta_1 \right.$$
$$\left. + \sqrt{(I_2 - I_1 + c)(c - I_2)} \cos \theta_2 \right]. \tag{2.9}$$

A *breather* is a solution of (2.1) that has the form $u_n = e^{-i\omega t} A_n$, with frequency ω real, and *breather amplitude* $A = [A_1, \ldots, A_N] \in \mathbf{C}^N$. Breathers are therefore periodic orbits of (2.1) that are also orbits of the action of global phase change. The action of global phase change on a breather solution yields another breather solution, moreover if $e^{-i\omega t} A$, $A \in \mathbf{C}^N$, $A_n \neq 0$, $\forall n \in \iota_N$, is a breather with $P(A) = Nc$, and $\bar{I}(A) = [I_1(A), \ldots, I_{N-1}(A)] \in \mathsf{S}_c^{N-1}$ is defined as the solution of (2.5) with $J_n = |A_n|$, $n \in \iota_N$, then $\bar{I}(A)$ is a fixed point of the reduced system (2.7). (The action $\bar{I}(A)$ of breathers with $A_k = 0$ for some $k \in \iota_N$ falls in the boundary of S_c^{N-1}.) Conversely, each fixed point I_0 of (2.7) in $\mathsf{S}_c^{N-1} \times \mathbf{T}^{N-1}$ corresponds to a circle of breather solutions of (2.1). More details on the above general facts on breathers, e.g. how to recover the frequency ω from the fixed point of the reduced system, can be found in [7]. There are many theoretical and numerical results on the existence of breathers for (2.1) and related discrete NLS equations in other lattices; see e.g. [6,13]. They are discussed further below.

Remark 2.2. By (2.7) breathers also correspond to the critical points of h_c on $\mathcal{M}$. Clearly, h_c can be defined in $\overline{\mathcal{M}}$ without reference to any particular coordinate system. We can apply the general theory of symplectic reduction to see that the fixed points of the reduced system are the critical points of h_c, moreover these fixed points correspond to breather periodic solutions; see [6, Chapter 4.3]. A smooth function on $\mathbf{CP}^{N-1}$ has at least N critical points, see e.g. [14], we thus have at least N breather solutions (up to a global sign flip) for all δ. The smoothness of the extension of h_c to $\overline{M}$ is a useful consequence of the general theory that is not obvious from the coordinate approach.

The stability of breathers can be studied by examining the stability of the fixed points of the reduced systems (2.7). Most of the literature on the stability of breathers uses a related alternative point of view, where breathers are seen as fixed point of the (2.1) in a suitable moving frame; see e.g. [13]. The relation between some of the results of these two approaches is discussed in the Appendix.

To examine the breathers of the $N = 3$ lattice we continue breathers of the (2.1) system with $\delta = 0$, "the anticontinuous limit" system; see e.g. [15]. In [7] we saw that for $\delta \neq 0$, $|\delta|$ sufficiently small, all breather solutions A satisfying $P(A) = C$ are, up to a global phase, continuations of real solutions of the $\delta = 0$ system. Given $C > 0$, real breathers of (2.1) with $\delta = 0$ are of the form

$$A_n = \pm \sqrt{\frac{\omega}{2}}, \quad \text{for } n \in U; A_n = 0, \text{ for } n \in U^c; \omega = \frac{2C}{|U|} \tag{2.10}$$

where $U \subset \iota_N$, and $|U|$ is the cardinality of U. Each breather of (2.1) with $\delta = 0$ may be represented by an array of the form $(s_1, \ldots, s_N)$, where $s_n = +(-)$, if $A_n > 0 (< 0)$, and $s_n = 0$ if $A_n = 0$. This representation holds for all breathers obtained for $|\delta|$ sufficiently small, and there is numerical evidence that we can use it to label breathers obtained for arbitrary δ; see [7] and the discussion of Fig. 1 below. Breathers related by a global sign flip correspond to the same fixed point of the reduced system.

In Fig. 1 we see δ vs. the energy E (the value of h_c) for all breather branches continued from the $\delta = 0$ breathers. Branches are continuous curves of breathers with amplitude $A \in \mathbf{R}^N$ in $\mathbf{R}^N \times (-\infty, 0]$ starting from $\mathbf{R}^N \times \{0\}$ and ending by colliding to another
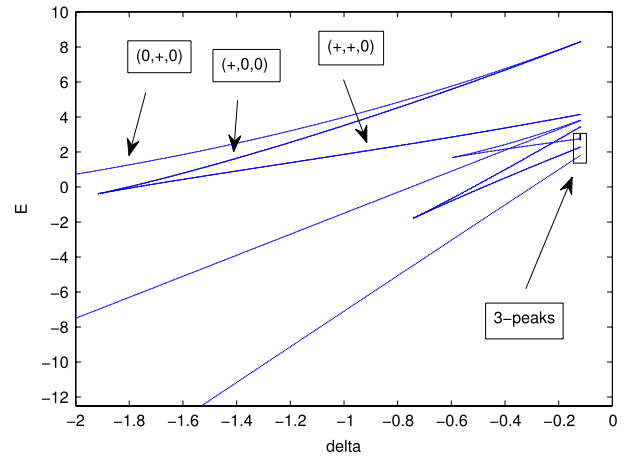

Fig. 1. δ vs. energy E for all breather branches continued from the $\delta = 0$ breathers.

continuous curve of solutions or extending to infinity. The figure suggests that all branches can be labeled by the $\delta = 0$ breather. We see that for $\delta < 0$ the largest energy corresponds to the breathers $(0, \pm, 0)$, while the smallest energy corresponds to the breathers $(\pm, t, \pm)$. (Global sign flip leaves the energy invariant.) For $\delta = 0$ the energies of all breathers with the same number of peaks coincide, moreover the energy is a decreasing function of the number of peaks. For $\delta \neq 0$ the energies of breathers with the same number of peaks in the $\delta \to 0$ limit generally differ. The box in the right of Fig. 1 shows all 3-peak breather branches near $\delta = -0.1$, and it is seen that their energies already differ noticeably. In comparison, the energies of the one-peak breather branches at the top are much closer to each other for this value of δ. Fig. 1 also shows several collision of branches as $|\delta|$ increases, e.g. the collision of branches $(\pm, 0, 0)$, $(\pm, \pm, 0)$, as well as three branches (up to global sign flip) that persist. These observations are discussed further and partially explained in [7,10]. For $\delta > 0$ we have analogous results, although the signs and ordering the energies of the different breathers are reversed, in particular localization decreases the energy. Note that a qualitatively similar figure is obtained in [9] for the saturable nonlinearity.

For $|\delta|$ sufficiently small Fig. 1 gives us all breather branches and therefore all the critical values of h_c on the reduced phase space. For such δ the spectra of $J\mathcal{H}$, $\mathcal{H}$ can be also computed analytically using the procedure described in [16] and it should be in principle possible to check the nondegeneracy of $\overline{H}$ analytically. In practice we study the spectra of $J\mathcal{H}$, $\mathcal{H}$, and $\overline{\mathcal{H}}$ numerically.

The reduced Hessian $\overline{\mathcal{H}}$ at the breathers $(0, \pm, 0)$, $(\pm, 0, 0)$, $(0, 0, \pm)$ has four negative eigenvalues, we thus verify that these breathers are local maxima of h_c. The corresponding Hessian $\mathcal{H}$ has four negative, one positive, and one zero eigenvalues, consistently with Proposition A.1. The breather $(0, \pm, 0)$ remains the global maximum for all $\delta < 0$. The energy of the $(\pm, 0, 0)$, $(0, 0, \pm)$ becomes slightly lower and they both remain nondegenerate local maxima until $\delta = \delta_* \approx -1.9$, when they collide with the $(\pm, \pm, 0)$, $(0, \pm, \pm)$ branches respectively. Note that the Hamiltonian is reflection invariant, where the reflection $\mathcal{R} : \mathbf{C}^N \to \mathbf{C}^N$ is defined by $\mathcal{R}$ by $(\mathcal{R}(A))_n = A_{N-n+1}$. The reduced Hessian $\overline{\mathcal{H}}$ at the breathers $(\pm, \pm, 0)$, $(0, \pm, \pm)$ has three negative and one positive eigenvalues, $\forall \delta \in (\delta_*, 0)$. The corresponding Hessian $\mathcal{H}$ has three negative, one positive, and one zero eigenvalues, consistently with Proposition A.1.

While we do not address the general problem of the topology of the energy hypersurfaces here, the above calculations suggest a guess of the critical energies corresponding to the passage from a disconnected to a connected energy hypersurface. We assume that Fig. 1 contains all the critical points of h_c and that h_c is smooth on

$\overline{\mathcal{M}}$; see Remark 2.2. The idea is to use $-h_c$ as a Morse function on $\overline{\mathcal{M}}$. Let $\mu(-E)$ denote the set of points $x \in \overline{\mathcal{M}}$ satisfying $-h_c(x) \leq -E$. The boundary $\partial\mu(-E)$ is the hypersurface of energy E. Let $\mathcal{A}_1(\delta)$ be any breather of the branches $(0, \pm, 0)$, at δ, and let $E_1(\delta) = h_c(\mathcal{A}_1)$. Define similarly the critical energies $E_2(\delta)$, $E_3(\delta)$ as the energies of any breathers of the branches $(\pm, 0, 0)$, $(\pm, \pm, 0)$ respectively at fixed δ respectively. For $\delta_* > \delta > 0$, Fig. 1 suggests that $E_1 > E_2 > E_3$, or $-E_1 < -E_2 < -E_3$. Fixing δ, and using the facts that E_1, E_2 are nondegenerate local maxima we use the Morse Lemma (Theorem 3.3, and Remark 3.3 of [12]), to argue that for $E \in (E_2, E_1)$ the set $\mu(-E)$ has the homotopy type of a closed 4-dimensional ball, while for $E \in (E_3, E_2)$ the set $\mu(-E)$ has the homotopy type of the union of three disjoint closed 4-dimensional balls. The hypersurface of energy E is then disconnected (we can also see directly from [12, Theorem 2.2], that $\mu(-E)$ is diffeomorphic to three disjoint closed 4-dimensional balls). By the computation of the spectrum of $\overline{\mathcal{H}}$, the Hessian of $-h_c$ at the critical value E_3 has index one. By the Morse Lemma, for $E < E_3$, E sufficiently near E_3, the set $\mu(-E)$ has the homotopy type of the union of three disjoint closed 4-dimensional balls with two one-cells attached.

One possibility is that the first cell connects the first ball to the second one, and the second cell connects the second ball to the third one, so that $\mu(-E)$ has the homotopy type of 4-cell and is connected so that its boundary can also be connected. A more refined argument (see the proof of Theorem 3.3 in [12]) would imply that $\mu(-E)$ is in fact diffeomorphic to a 4-dimensional closed ball and so that its boundary is connected.

To verify this scenario we integrate numerically backward in time the gradient flow of $-h_c$ along the one-dimensional stable manifolds of $(\pm, \pm, 0)$, $(0, \pm, \pm)$, or equivalently integrate the gradient flow of h_c along the unstable manifolds of $(\pm, \pm, 0)$, $(0, \pm, \pm)$. To define the gradient we use the metric g with components $g_{ij} = \delta_{ij}$ in the I, $\overline{\theta}$ system on $\overline{\mathcal{M}}$. Integrating ∇h_c numerically with initial conditions sufficiently near $(\pm, \pm, 0)$, and along the two sides of the unstable direction of $(\pm, \pm, 0)$, we obtain trajectories that converge to the breathers $(\pm, 0, 0)$, and $(0, \pm, 0)$ respectively. Likewise, integrating ∇h_c with initial conditions sufficiently near $(0, \pm, \pm)$, and along the two sides of the unstable direction of $(0, \pm, \pm)$, we obtain trajectories that converge to the breathers $(0, 0, \pm)$, and $(0, \pm, 0)$ respectively.

The above suggests that for energies below E_3 there is no energetic barrier to motions connecting the vicinities of the two-peak breathers $(\pm, \pm, 0)$, $(0, \pm, \pm)$ (at least in the vicinity of $\delta = -1.2$ and possibly in a wider range of δ). It is also interesting that the suggested connectivity of the energy hypersurface reflects the connectivity of the lattice. A related idea of an energy barrier to the mobility of breathers has been used by many authors; see e.g. [17,18] (we discuss this further in Section 4). The concept of an energy barrier seems clearer here; however it does explain how trajectories move in the larger energy hypersurface. To get some information on this problem we start from the observation that for $\delta \to 0^-$ the two-peak $(\ldots, \pm, \pm, \ldots)$ breathers of an N-site lattice, $N \geq 2$, have one stable and one unstable direction; see [16,7]. Assuming that this holds also for smaller δ we can examine one dimensional stable and unstable manifold of the invariant subsets in the center manifold of these breathers. In the next section we examine the simplest problem of this type for $N = 3$.

Remark 2.3. $\delta < 0$ corresponds to the "focusing" case, where the signs of the quadratic and quartic terms of H in (2.2) are opposite. In analogous PDE problems one can establish the existence of breathers by looking for minima of the analogue of the focusing $-H$ among certain classes of functions with constant power. Such minima are analogous to our maxima.

3. Lyapunov orbits and their instabilities

To study numerically the dynamics of trajectories starting near the unstable 2-peak breathers $(0, +, +)$, and $(+, +, 0)$ discussed in the previous section, we first outline some standard theoretical results.

Fix $\delta < 0$, and denote the corresponding vector field (2.7), (2.9) by X. Let $K \in \mathcal{M} = \mathbf{S}_c^2 \times \mathbf{T}^2$ be any one of the two fixed points K_L, K_R of X that correspond to the breathers $(0, +, +)$, $(+, +, 0)$ at δ. The linearization of X around K is assumed to have two elliptic and two hyperbolic directions, one stable, and one unstable, as is seen numerically. Denote the center, stable, and unstable subspaces by E_K^c, E_K^s, and E_K^u respectively and note that the reduced system (2.7) is C^∞ in $\mathcal{M}$. We then have the following statements about X.

Proposition 3.1. (i) *There exist unique C^∞ one-dimensional stable and unstable manifolds W_K^s, W_K^u of K respectively.* (ii) *There exists a C^∞ two-dimensional center manifold $W_K^c(\epsilon_*)$ of K.* (iii) $W_K^c(\epsilon_*) \setminus \{K\}$ *is foliated by a C^∞ one-parameter family of T_E-periodic orbits $\gamma_E : \mathbf{R} \to \mathcal{M}$, $E \in (E_3, E_3 - \epsilon_*)$. The parameter E is the energy, that is $h_c(\gamma_E) = E$; also $E_3 = h_c(K)$.* (iv) *The periodic orbits γ_E, $E \in (E_3, E_3 - \epsilon_*)$, are linearly unstable. Each γ_E, $E \in (E_3, E_3 - \epsilon_*)$, has unique C^∞ two-dimensional global stable and unstable manifolds $W_{\gamma_E}^s$ and $W_{\gamma_E}^u$ respectively.*

The periodic orbits γ_ϵ are referred to as *Lyapunov orbits*. We will view $W_K^c \setminus \{K\}$ as a union of Lyapunov orbits, and approximate it by constructing the Lyapunov orbits numerically.

Recall that W_K^s, W_K^u are invariant under the flow of X, moreover they consist of all points that approach K as $t \to \pm\infty$ respectively and are tangent to E_K^s, E_K^u respectively at K. Also, $W_K^c(\epsilon_*)$ is invariant under the flow of X and tangent to E_K^c at K. The proof of part (i) and the existence of a center manifold is standard; see e.g. [19]. The existence of the Lyapunov orbits can be shown by considering X as a Hamiltonian perturbation of its linearization around K. We can then continue the periodic orbits in a neighborhood of K in E^c by verifying condition on their Floquet spectrum and using the fact that X is conserves the energy; see e.g. [20, Chapters V, VI]. We check explicitly that the energies of periodic orbits of the linearized system decrease as we move away from K, this implies that the energies of the Lyapunov orbits also decrease from E_3 as we move away from K in $W_K^c(\epsilon_*)$. The Lyapunov orbits are hyperbolic on each energy hypersurface and we can use the Poincaré map to construct local stable and unstable manifolds for each γ_E, these can be extended to the $W_{\gamma_E}^s$ and $W_{\gamma_E}^u$ respectively, see e.g. [6, Chapter 7.2], for statements and references. Recall that $W_{\gamma_E}^s$ and $W_{\gamma_E}^u$ consist of all points that approach γ_E as $t \to \pm\infty$ respectively. They are also invariant under the flow.

The above statements give a complete picture of the neighborhood of each periodic orbit γ_E on the corresponding energy hypersurface $\mathcal{S}_E = \{x \in \mathcal{M} : h_c(x) = E\}$, and in a neighborhood of $\cup_{E \in [E_3, E_3 - \epsilon_*]} \gamma_E$. Further away from γ_E in $\mathcal{S}_E$, $W_{\gamma_E}^s$, $W_{\gamma_E}^u$ may intersect transversely at a manifold of dimension one since each is of dimension two and $\mathcal{S}_E$ is of dimension three. Since these considerations apply to both fixed points K_L, K_R and we also look for intersections $W_{\gamma_E}^s \cap W_{\gamma_E'}^u$, $W_{\gamma_E}^u \cap W_{\gamma_E'}^s$, where $K = K_L$, γ_E, γ_E' the Lyapunov orbits of energy E around K_L, K_R respectively.

In the numerical study below the main step in approximating $W_{\gamma_E}^s$, $W_{\gamma_E}^s$ is the numerical computation of the Lyapunov orbits. To compute these orbits we use a Poincaré section near K and look for fixed points of the return map restricted to an energy hypersurface. The values of the return map are computed numerically and we find fixed points using Powell's hybrid Newton method with a numerically approximated derivative; see [21]. A fixed point then yields a periodic orbit of prescribed energy, and the procedure is repeated for other values of the energy. Some details are provided

below. The question of maximal extension of W_K^c is not considered here. Our algorithm fails to converge below some energy. This is discussed at the end of the section.

Once we have the Lyapunov orbits we approximate their stable and unstable manifolds by integrating numerically starting from initial conditions $x + \epsilon v^s$, $x + \epsilon v^u$, where x is a point in the computed Lyapunov orbit γ_E, v^s, v^u are unit vectors on the stable, and unstable subspace of the fixed point K, and $|\epsilon| \ll 1$. Varying x along the computed γ_E and integrating backwards or forwards starting from $x + \epsilon v^s$, $x + \epsilon v^u$ we obtain approximations of two-dimensional "cylinders" $W_{\gamma_E}^s$, $W_{\gamma_E}^u$. We are thus assuming that the stable and unstable directions of the Lyapunov orbits are close to the stable and unstable directions of the fixed point. A similar simplification was used in [11]. A more refined calculation of the $W_{\gamma_E}^s$, $W_{\gamma_E}^u$ uses instead trajectories starting from $x + \epsilon w^s(x)$, $x + \epsilon w^u(x)$, where the $w^s(x)$, $w^u(x)$ are unit vectors along the stable and unstable directions of the Floquet map at $x \in \gamma_E$. The results presented below were obtained using the first approach, but as we discuss at the end of the section, the second approach gives essentially the same results. This is probably due to the fact that trajectories starting near the $w^u(x)$, $w^s(x)$, e.g. in cones around them, move closer to $W_{\gamma_E}^s$, $W_{\gamma_E}^u$ as we integrate (backwards and forwards respectively). It is also reasonable to expect that transverse intersections of the computed cylinders, assumed to be exact invariant manifolds of the flow of energy E, imply the intersection of nearby cylinders the are subsets of the $W_{\gamma_E}^s$, $W_{\gamma_E}^u$. The assumption of transversality may be substituted by some other topological continuation argument. In what follows we use the same notation for both the exact and numerical γ_E, $W_{\gamma_E}^s$, $W_{\gamma_E}^u$.

Note that the energy of the initial conditions $x + \epsilon v^s$, $x + \epsilon v^u$, $x \in \gamma_E$, is not exactly E; this discrepancy is minimized by decreasing $|\epsilon|$. In practice we see that for $|\epsilon|$ sufficiently small the absolute value of ϵ does not affect the trajectory significantly. Also, each of $W_{\gamma_E}^s \setminus \gamma_E$, $W_{\gamma_E}^u \setminus \gamma_E$ consists of two disjoint half-cylinders that we denote respectively by $W_{\gamma_E}^s(j)$, $W_{\gamma_E}^u(j)$, $j = 1, 2$. We have seen that to produce clear pictures of $W_{\gamma_E}^s$, $W_{\gamma_E}^u$ we need initial conditions that belong to the same half-cylinder. To do that we use $x \in \gamma_E$, and choose a particular half-cylinder by fixing the sign of ϵ. Integration from initial conditions $x + \epsilon v^s$, $x + \epsilon v^u$, with x in a periodic orbit of the linearization (on E_K^c) yields trajectories that in general seem to belong to different half-cylinders, i.e. the simplest approximation of the γ_E does not seem sufficient and we need to compute γ_E.

We also examine the intersection of the cylinders $W_{\gamma_E}^s$, $W_{\gamma_E}^u$ with three dimensional hypersurfaces Σ (Poincaré sections) in $\mathcal{M}$ that we choose. Nonempty transverse intersections $\Sigma \cap W_{\gamma_E}^s$, $\Sigma \cap W_{\gamma_E}^u$ are one-dimensional, moreover $W_{\gamma_E}^s \cap \Sigma$, $W_{\gamma_E}^u \cap \Sigma$ can intersect at points. To visualize these intersections better we also study intersections of discs $\tilde{D}_{\mathcal{E}}^s = \Sigma \cap (\cup_{E \in \mathcal{E}} W_{\gamma_E}^s)$, $\tilde{D}_{\mathcal{E}}^u = \Sigma \cap (\cup_{E \in \mathcal{E}} W_{\gamma_E}^u)$, with $\mathcal{E}$ an interval of energies in $(E_3 - \epsilon_*, E_3)$. These discs in Σ can intersect transversely along curves.

It may be expected that the cylinders $W_{\gamma_E}^s$, $W_{\gamma_E}^u$ "follow" the stable and unstable manifolds W_K^s, W_K^u of K. These are computed by integrating backwards and forwards from an initial condition $K + \epsilon v^s$, $K + \epsilon v^u$, with $v^s \in W_K^s$, $v^u \in W_K^u$, $|\epsilon|$ small. To visualize we project the W_K^s, W_K^u to the plane of the actions. We observe that the projections coincide. This follows from the elementary fact that phase conjugation is equivalent to time reversal.

Proposition 3.2. *Let B be a fixed point of the reduced system* (2.7) *in* $S_c^{N-1} \times \mathbf{T}^{N-1}$, *and let* W_B^s, W_B^u *be the corresponding stable and unstable manifolds of B. Let* $Proj(\bar{I}, \bar{\theta}) = \bar{I}$ *for* $(\bar{I}, \bar{\theta}) \in S_c^{N-1} \times \mathbf{T}^{N-1}$. *Then* $Proj(W_B^s) = Proj(W_B^u)$.

Proof. Writing (2.1) as $\dot{u} = F(u)$, $u(t)$ at a trajectory in $\mathbf{C}^N$, $F: \mathbf{C}^N \to \mathbf{C}^N$ we observe that the conjugate u^* satisfies $\dot{u}^* = -F(u^*)$. Thus $y \in W_B^s$ implies $y^* \in W_B^u$, for every fixed point B. $\square$
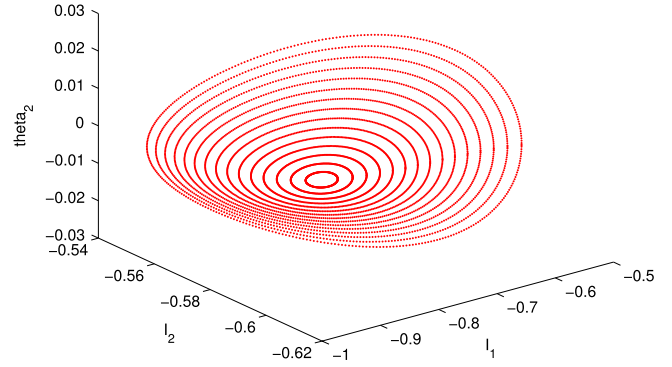

Fig. 2a. I_1, I_2, θ_2 (right, left, vertical axes resp.) components of Lyapunov orbits around breather $(0, +, +)$ at $\delta = -1.2$ ($c = 1$).
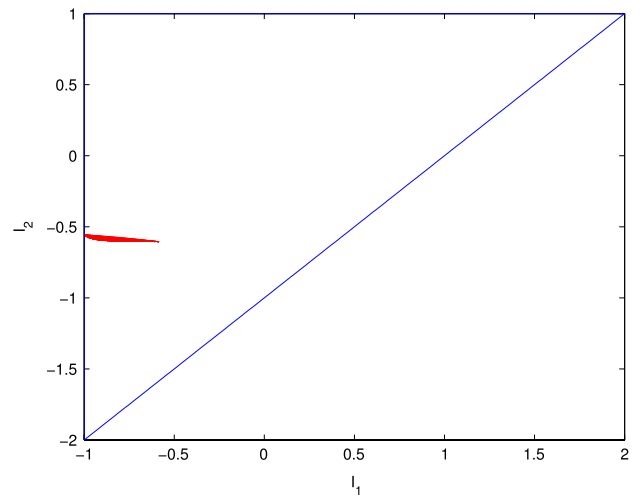

Fig. 2b. Projection of Lyapunov orbits of Fig. 4a to I_1, I_2 plane.

To compute the Lyapunov orbits around the breather $K \in \mathcal{M} = S_c^2 \times \mathbf{T}^2$, we work in the covering space $S_c^2 \times \mathbf{R}^2$ of $\mathcal{M}$, which we view as a subset of $\mathbf{R}^4$. X extends to $S_c^2 \times \mathbf{R}^2$ by periodicity in the angles. We compute an orthonormal basis $\{\hat{v}_1, \hat{v}_2\}$ of $E_K^c \subset \mathbf{R}^4$, and augment it to an orthonormal basis $\{\hat{v}_1, \hat{v}_2, \hat{w}_1, \hat{w}_2\}$ of $\mathbf{R}^4$. We consider the set Σ_0 of all $z = K + x_1 \hat{v}_1 + y_1 \hat{w}_1 + y_2 \hat{w}_2$, satisfying $x_1 > 0$, $y_1, y_2 \in \mathbf{R}$, and $z \in S_c^2 \times \mathbf{R}^2$. The set Σ_0 will be used as a Poincaré section. Note that Σ_0 intersects $K + E_K^c$ along points of the form $x_1 \hat{v}_1$, with $x_1 > 0$. To compute the Lyapunov orbit γ_E, let $y = (y_1, y_2) \in \mathbf{R}^2$ and compute numerically a $x_1(y) > 0$ for which $z(y) = K + x_1(y) \hat{v}_1 + y_1 \hat{w}_1 + y_2 \hat{w}_2 \in \Sigma$ satisfies $h_c(z) = E$. It is assumed that such x_1 is unique, this can be verified for y sufficiently near the origin. Integrate numerically X from the initial condition $z(y)$ until the trajectory intersects Σ_0 for the first time at some time $\tau > 0$ at some point $z'(y)$. We can check that trajectories leave Σ_0 for $t > 0$, and thus the first return time τ is well defined. $z'(y)$ can be written uniquely as $z'(y) = K + x_1' \hat{v}_1 + y_1' \hat{w}_1 + y_2' \hat{w}_2$, and we let $\mathcal{F}_E(y) = y' = (y_1', y_2')$. If $y^* = (y_1^*, y_2^*)$ is a fixed point of $\mathcal{F}$ then the unique point $z = K + x_1(y^*) \hat{v}_1 + y_1^* \hat{w}_1 + y_2^* \hat{w}_2 \in \Sigma$ satisfying $h_c(z) = E$ belongs to the periodic orbit γ_E.

An example of numerical Lyapunov orbits around $K = (0, +, +)$ at $\delta = -1.2$ is shown in Fig. 2a, where we show the I_1, I_2, θ_2 components. The average power is $c = 1$. The energy of the breather is 1.388352992 and we show 15 periodic orbits with energies ranging from $E = 1.385148006$ to 1.051336388, with the energy decreasing as we go outwards. For $\delta = -1.2$ the Newton iteration fails to converge at $E \approx 0.92$. In Fig. 2b we show the
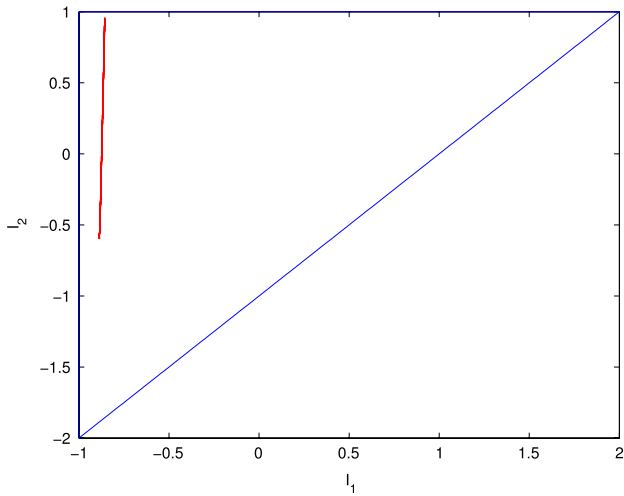
Fig. 3a. Projection of segment of W_K^u onto I_1, I_2 plane. K is breather $(0, +, +)$ at $\delta = -1.2\,(c = 1)$.

Fig. 3b. Details of Fig. 5(a).

projection of the orbits of Fig. 1 to the I_1, I_2 plane. Note that the breather is at $[I_1, I_2] = [-0.886395065, -0.596179304]$. A similar result is obtained for the breather $(+, +, 0)$; the projection is the shape of Fig. 2b, reflected by the antidiagonal $I_2 = -I_1$.

By Fig. 2b the projections of the periodic orbits and W_K^c in S_c^2 are roughly horizontal. We also see numerically that the projection of the stable and unstable subspace E_K^s to S_c^2 points roughly in the vertical direction (by Proposition 3.2 the projections of E_K^s, E_K^u onto S_c^2 coincide since projection is differentiable). We integrate forward starting from points $x - 10^{-2}v^u$, $x \in \gamma_E$ to obtain an approximation of the half-cylinder $W_{\gamma_E}^u(1) \subset W_{\gamma_E}^u$. Also we integrate backwards starting from points $x + 10^{-2}v^s$, $x \in \gamma_E$ to obtain an approximation of the half-cylinder $W_{\gamma_E}^s(1) \subset W_{\gamma_E}^s$. The dependence of the $W_{\gamma_E}^u(1)$, $W_{\gamma_E}^s(1)$ on the integration interval is not made explicit in the notation. The signs of the scalars multiplying v^s, v^u are specific to the v^s, v^u we choose. The projections of the $W_{\gamma_E}^u(1)$, $W_{\gamma_E}^s(1)$ onto S_c^2 are seen to roughly lie above the projection of W_K^c. The projection of the time-t map of each set of initial conditions $\gamma_E - 10^{-2}v^u$, $\gamma_E + 10^{-2}v^s$ remains roughly horizontal and moves back and forth (i.e. up and down) between the shape of Fig. 2b and the horizontal side of the triangle S_c^2 (corresponding to $|u_2| = 0$). This motion is seen over an interval of integration that is about 15 times the average period of the periodic orbits. During that time the trajectories return to the vicinity of γ_E four times. This rough picture is more apt for the inner orbits, as these are seen to follow the stable and unstable manifolds W_K^s, W_K^u closely, spiraling around them. In Fig. 3a we show the projection of a segment of W_K^u onto S_c^2 obtained by integrating forward from $K - 10^{-3}v^u$. The time interval is as for Fig. 2b. The lowest point of the apparent linear segment is near the fixed point K. The trajectory starts near K and moves back and forth between the vicinity of K and the horizontal side of S_c^2. In Fig. 3b we zoom Fig. 3a near K and see four returns to the vicinity of K. W_K^u does not appear to be a homoclinic orbit; its minimum distance from K at each near-return in Fig. 3b is small, $\sim 10^{-2}$ in the actions, but nonzero within the accuracy of the numerical integration.

Given a set of computed periodic orbits γ_E, $E \in \mathcal{E}$, we examine intersections of collections of half-cylinders $\cup_{E \in \mathcal{E}} W_{\gamma_E}^u(1)$, $\cup_{E \in \mathcal{E}} W_{\gamma_E}^s(1)$ with a section Σ_1 defined by $I_1 + I_2 + 0.2 = 0$. The tubes can intersect Σ_1 many times and in Figs. 4a and 4b we show the second intersection $D_{\mathcal{E}}^u(1, 2)$ of $\cup_{E \in \mathcal{E}} W_{\gamma_E}^u(1)$ with Σ_1 in Σ_1, and the first intersection $D_{\mathcal{E}}^s(1, -1)$ of $\cup_{E \in \mathcal{E}} W_{\gamma_E}^s(1)$ with Σ_1 in Σ_1. Σ_1 has coordinates θ_1, I_2, θ_2, and we are zooming at the intersections corresponding to the innermost periodic orbits.
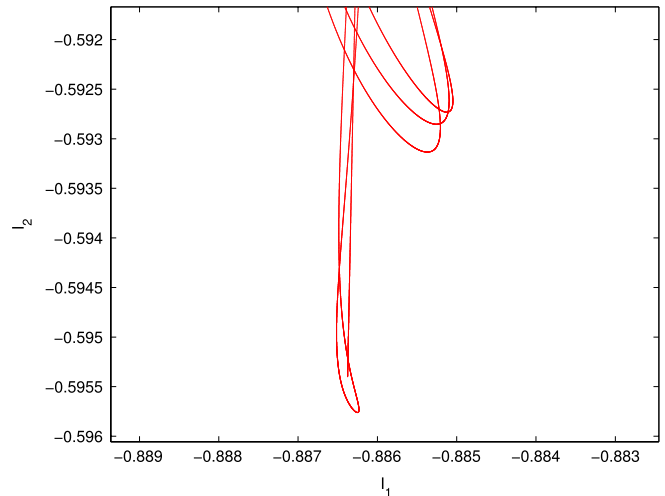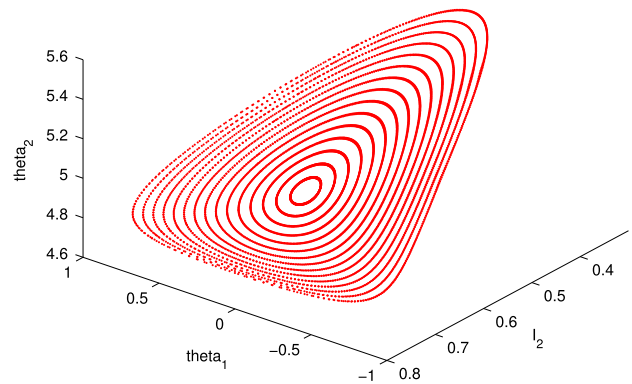

Fig. 4a. I_2, θ_1, θ_2 components (right, left, vertical axes resp.) of first intersection $\cup_{E \in \mathcal{E}} W_{\gamma_E}^u(1)$ with Σ_1 and second intersection of $\cup_{E \in \mathcal{E}} W_{\gamma_E}^s(1)$ with Σ_1.
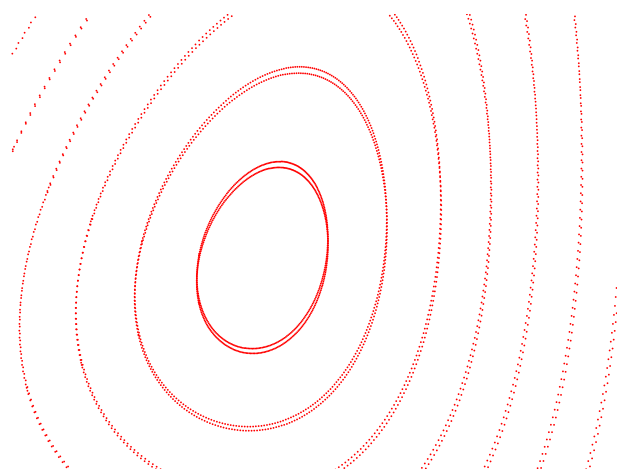

Fig. 4b. Details of Fig. 6(a).

Note that the first intersection of $\cup_{E \in \mathcal{E}} W_{\gamma_E}^u(1)$ with Σ_1 occurs when the trajectories cross Σ_1 while moving upwards toward the horizontal side of the triangle, while the second occurs shortly thereafter as the trajectories are starting move downwards, toward the vicinity of the periodic orbits of Fig. 4b. In Fig. 4a we plot both surfaces $D_{\mathcal{E}}^u(1, 2)$, $D_{\mathcal{E}}^s(1, 1)$. Visual inspection suggests that
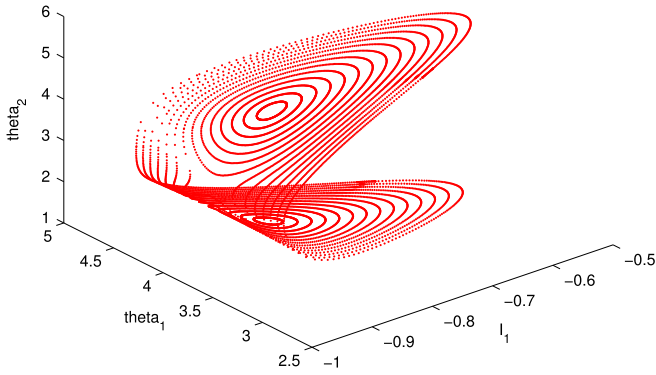
Fig. 5. I_1, θ_1, θ_2 components (right, left, vertical axes resp.) of first and second intersections of $\cup_{E \in \mathcal{E}} W^s_{\gamma_E}(1)$ with Σ_2.

Fig. 6. Projection of segment of W^s_K onto I_1, I_2 plane. K is breather $(0, +, +)$ at $\delta = -1.2$ $(c = 1)$.

the surfaces (and the circles on them) almost coincide, and are almost flat. In Fig. 4b we zoom at the innermost circles and see that the circles from $W^u_{\gamma_E}(1)$, $W^s_{\gamma_E}(1)$ are slightly different, intersecting at two points. These points should correspond to homoclinic orbits of the corresponding periodic orbits. These small differences are consistent with the small but nonzero difference we also see between the second intersection of W^u_K with Σ_1 and the first intersection of W^u_K with Σ_1.

In Fig. 5 we show the first and second intersections of $\cup_{E \in \mathcal{E}} W^s_{\gamma_E}(1)$ with Σ_2 defined by $I_1 + I_2 = 0$. For the larger energies, corresponding to the innermost circles of initial conditions, we see two intersections of $W^s_{\gamma_E}(1)$ with Σ_2. For smaller energies we see trajectories that intersect Σ_2 twice, and trajectories that do not intersect Σ_2 at all. Examining the projections of the flow of each outer circle of initial conditions to S^2_c, we see that one part of the circle does not go near the horizontal side of the triangle and starts to move downwards while another part of the circle continues to move upwards and returns downwards later. The first part does not intersect Σ_2, while the second part crosses Σ_2 both when it moves upwards, and when it returns. For the inner circles we see that all their points cross Σ_2 twice.

Similarly, we integrate forward starting from points $x + 10^{-2}v^u$, $x \in \gamma_E$, to obtain an approximation of the half-cylinder $W^u_{\gamma_E}(2) \subset W^u_{\gamma_E}$. Also we integrate backwards starting from points $x - 10^{-2}v^s$, $x \in \gamma_E$ to obtain an approximation of the half-cylinder $W^s_{\gamma_E}(2) \subset W^s_{\gamma_E}$. The projections of these trajectories onto S^2_c stay roughly below the Lyapunov orbits. This is indicated in Fig. 6 where we show the segment of W^u_K onto S^2_c obtained by integrating forward from $K + 10^{-3}v^u$. The integration time is the same as in Figs. 3a and 3b. In Fig. 6 we see many excursions to the vicinity of the diagonal side of the action triangle (corresponding to $|u_1| = 0$), with more frequent but less close returns to the vicinity of the fixed point. Also, projection of the trajectory stays below the fixed point. We further examine intersections of collections of half-cylinders $\cup_{E \in \mathcal{E}} \tilde{W}^u_{\gamma_E}(2)$ and $\cup_{E \in \mathcal{E}} \tilde{W}^s_{\gamma_E}(2)$, γ_E, $E \in \mathcal{E}$, with the hypersurface Σ_3 defined by $I_2 + 1.5 = 0$. In Fig. 7 we show the first intersection $\tilde{D}^u_{\mathcal{E}}(2, 1)$ of $\cup_{E \in \mathcal{E}} \tilde{W}^u_{\gamma_E}(2)$ with Σ_3 in Σ_3, and the second intersection $\tilde{D}^s_{\mathcal{E}}(2, -2)$ of $\cup_{E \in \mathcal{E}} \tilde{W}^s_{\gamma_E}(2)$ with Σ_3 in Σ_3. Σ_3 has coordinates I_1, θ_1, θ_2. The figure indicates that the discs $\tilde{D}^u_{\mathcal{E}}(2, 1)$, $\tilde{D}^s_{\mathcal{E}}(2, -2)$ intersect transversely in Σ_3. Further visual inspection using different projections suggests that the intersection occurs at the outer circles only. (This may not be as clear from Fig. 7 or any particular projection but becomes clearer by comparing different projections.) We thus see evidence for trajectories that are homoclinic to some of the γ_E.

Similar results are obtained when $K = (+, +, 0)$. We can also compare stable and unstable manifolds of Lyapunov orbits around
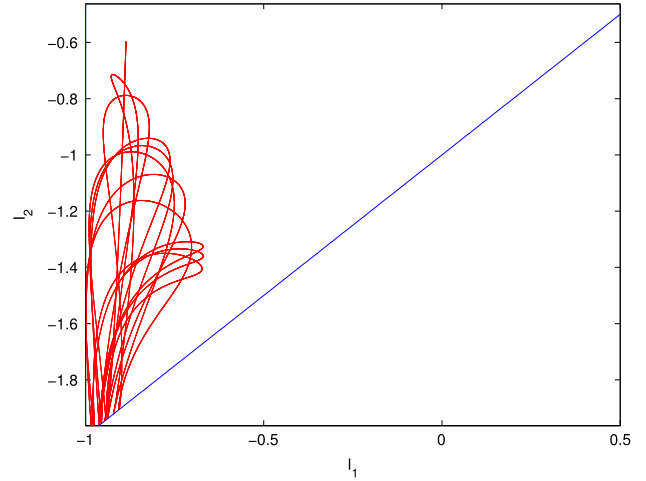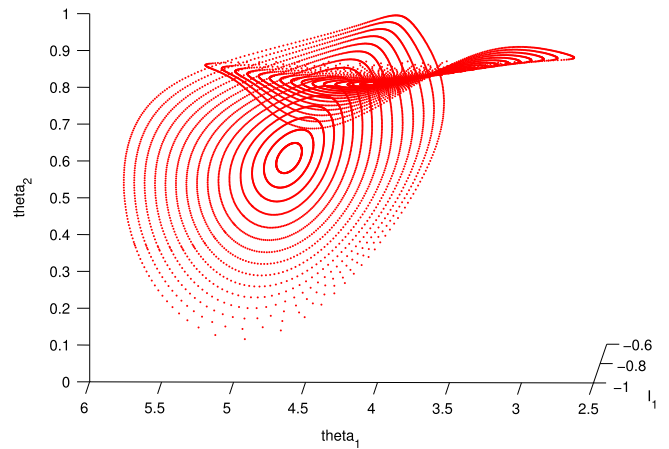

Fig. 7. I_1, θ_1, θ_2 components (right, left, vertical axes resp.) of first intersection of $\cup_{E \in \mathcal{E}} \tilde{W}^u_{\gamma_E}(2)$ with Σ_3 and second intersection of $\cup_{E \in \mathcal{E}} \tilde{W}^s_{\gamma_E}(2)$ with Σ_3.

K_L, and K_R. Fixing a range of energies $\mathcal{E}$, we denote a Lyapunov orbits of energy $E \in \mathcal{E}$ around K_L, K_R by γ_E, γ'_E respectively. We compare $\Sigma_2 \cap (\cup_{E \in \mathcal{E}} W^u_{\gamma_E}(1))$ to an analogous intersection $\Sigma_2 \cap (\cup_{E \in \mathcal{E}} W^s_{\gamma'_E}(1))$, $E \in \mathcal{E}$ obtained by starting from the vicinity of γ'_E and integrating backwards. In Fig. 8 we consider orbits in $\mathcal{E} = [1.051336388, 1.385148006]$ (as in Figs. 2a and 2b) we show the first and second intersections of $\cup_{E \in \mathcal{E}} W^u_{\gamma_E}(1)$ with Σ_2 in Σ_2 (also shown in Fig. 5), and the first and second intersections of $\cup_{E \in \mathcal{E}} W^s_{\gamma'_E}(1)$ with Σ_2 in Σ_2. While the distance between the first and second intersections of $\Sigma_2 \cap W^u_{\gamma_E}(1)$ and $\Sigma_2 \cap W^s_{\gamma'_E}(1)$ decreases as we decrease E, we do not see any intersection. For $E \approx 0.92$ the numerical iteration for the Lyapunov orbits fails to converge and the picture is essentially as in Fig. 8. Similar results are obtained for the third and fourth intersections of $\Sigma_2 \cap W^u_{\gamma_E}(1)$, $\Sigma_2 \cap W^s_{\gamma'_E}(1)$ with Σ_2. The circles are distorted significantly but still fall into the two dimensional shapes of Fig. 8, and the trajectories originating from the vicinities of γ_E, γ'_E stay apart. (Some trajectories intersect more that twice but less that four times with Σ_2 in the time interval considered.) We therefore do not see any evidence for heteroclinic connections between γ_E, γ'_E for the energy range considered and time scale of the first few intersections. Intersections must occur for larger time scales, or lower energies, if at all.
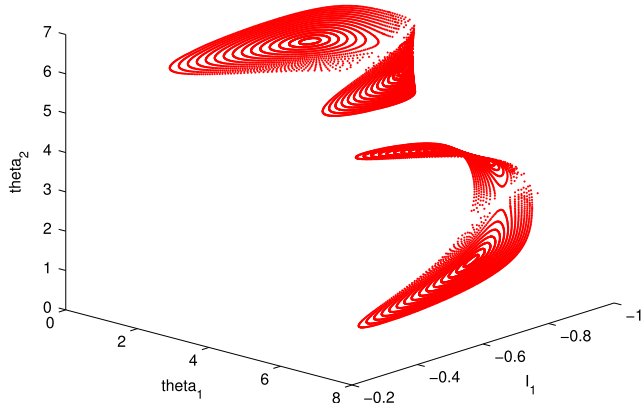
Fig. 8. I_1, θ_1, θ_2 components (right, left, vertical axes resp.) of first and second intersections of $\cup_{E\in\mathcal{E}} W^s_{\gamma_E}(1)$ with Σ_2, and first and second intersections of $\cup_{E\in\mathcal{E}} W^s_{\gamma'_E}(1)$ with Σ_2.

The lack of heteroclinic connections between γ_E, γ'_E for E near the energy of the breathers K, K' is consistent with the numerical observation that $\Sigma_2 \cup W^u_K$, $\Sigma_2 \cup W^s_{K'}$ have different angle components (their action components coincide). If we denote the angle components of the n-th intersections $y \in \Sigma_2 \cup W^u_K$, $y' \in \Sigma_2 \cup W^s_{K'}$ by (Θ_1, Θ_2), $(\tilde\Theta_1, \tilde\Theta_2)$ respectively, we can use reflection symmetry arguments to see that $y' = \mathcal{R}y$, and $\tilde\Theta_1 = -\Theta_2$, $\tilde\Theta_2 = -\Theta_1$. (The reflection operation $\mathcal{R}$ was defined earlier and commutes with the flow of (2.1).) In the numerical examples we saw that Θ_1, Θ_2 stay away from zero. The stable and unstable manifolds therefore stay apart.

The above results are corroborated by a computation of the $W^s_{\gamma_E}$, $W^u_{\gamma_E}$ that uses integration from the $x + \epsilon w^s(x)$, $x + \epsilon w^u(x)$, $x \in \gamma_E$. The normalized stable and unstable directions $w^s(x), w^u(x)$ of the Floquet map at each $x \in \gamma_E$ are computed by integrating the variational equation, and ϵ is as in the corresponding calculations with initial conditions $x+\epsilon v^s, x+\epsilon v^u$. Comparing the intersections $\Sigma \cap W^s_{\gamma_E}$, $\Sigma \cap W^u_{\gamma_E}$ for the Poincaré sections Σ of Figs. 5, 7, 4a and 4b we see that the times and points of intersection obtained by the two methods are very close, typically to 10^{-3}–10^{-4}, so that the corresponding circles and discs are indistinguishable at the scale of the figures. This is especially remarkable in the case of Figs. 4a and 4b, where magnification shows the intersections of circles of Fig. 4b. We also checked numerical integration using smaller time steps leads to the same results. Thus the two methods of approximating the stable and unstable manifolds of the Lyapunov orbits yield the same qualitative results. Their comparison also suggests that the objects we compute are robust.

Regarding the observed failure of convergence of the computation of the Lyapunov orbits γ_E below an approximate apparent energy threshold E_*, we first note that the computations of the γ_E appear to be accurate up until E_*. For instance the Floquet spectrum of the γ_E, computed by integrating the variational equation with time step 10^{-3}, has two unit eigenvalues, as expected, up to an accuracy 10^{-4}. Moreover the accuracy of the unit eigenvalues can be improved further by reducing the time step. As the energy is decreased to E_*, we see that the distance between the γ_E and the singular set $I_1 = -c$ decreases, and that the orbits spend a larger portion (up to about 8%) of their period in the vicinity of $I_1 = -c$, where the vector field becomes singular. The period of the γ_E does not change significantly as we approach E_*, moreover the remaining eigenvalues $\lambda > 1, \lambda^{-1}$ of the Floquet spectrum remain far from unity, e.g. $\lambda > 50$ for the orbits of Figs. 4a and 4b. The apparent hyperbolicity of the γ_E as we approach E_* suggests that we should be able to continue the orbits uniquely beyond E_*, see e.g. [20, Chapter

V, Section E]. The possibility of a smooth fold at E_* is also not likely, as the slopes of the $y_j(E)$ remain bounded in absolute value, and in fact seem to vanish, as we approach E_*. (By Fig. 1, E_* is also far above the energy of the next breather.) The above seem to imply that the failure of the algorithm does not imply any bifurcations, and is more likely due the difficulty in integrating precisely in the vicinity of the singular set our coordinate system.

4. Discussion

There are several remaining questions on the 3-site NLS lattice system we considered. The system is apparently far from one with known homoclinic or heteroclinic connections, so that theoretical results on the continuation of such orbits, e.g. see [22, p. 462], do not seem applicable. Regarding homoclinic connections, we can consider a lattice of two sites (the sites $n = 1, 2$) that is weakly coupled to a third site. The phase space of the two site system has a $(\pm, \pm)$ unstable orbit (see [7]), while the third site is an anharmonic oscillator. We may then expect some persistence results on the intersections of stable and unstable manifolds of the Lyapunov orbits of the uncoupled system. It is worth examining whether such possible intersections persist as we bring the couplings closer to the ones here.

It is also natural to try to connect the local dynamics of breathers to questions on energy transport in lattices, even though larger lattices may have significantly different properties and what was seen here is not as relevant. In any case, the notions of instability and change in the connectivity of the energy hypersurface are meaningful for larger lattices and should be investigated further. Note that breather mobility is often studied by reducing the problem to the planar Hamiltonian system of the pendulum; see [17]. This approach can be very useful, but we see here that having a connected energy hypersurface in the full system does not imply a similar simple scenario of energy transport. We do not know whether the notions of energy hypersurface connectivity and mobility barrier for simplified planar models become comparable in larger lattices. Also, one can move a one-peak breather with initial condition A by multiplying it by a "phase", e.g. e^{ikn}; see [23]. The new initial condition has the same power and a smaller energy than A (for the choice of signs used here) so that the energy considerations here should be relevant. We also note that [24] propose a mechanism for breather mobility that in the context of NLS type equations seems to require the collision of imaginary eigenvalues of $J\mathcal{H}$ of (A.2). Such collisions do occur for some breathers of (2.1), see [10], but not for the two-peak breathers in $N = 3$. It is not clear that such collisions are related to changes in the connectivity of the energy hypersurface. Some of these possible connections between mobility and breathers will be examined in further work.

Appendix

To study the stability of breathers we consider a breather solution $u = e^{-i\omega t}A$ of (2.1), and define v by $u = e^{-i\omega t}v$. Then v satisfies Hamilton's equations

$$\dot v_n = -i\frac{\partial H_\omega}{\partial v_n^*}, \quad n \in \mathbf{Z}^d, \text{ with } H_\omega = H - \omega P, \qquad (A.1)$$

with H as in (2.2), and P the power. Furthermore $v = A$ is a fixed point of (A.1) and we examine the linearization of (A.1) around A. Let $w = [Q_1, \ldots, Q_n, P_1, \ldots, P_n]^T \in \mathbf{R}^{2N}$, $h_\omega = \frac{1}{2}H_\omega$, $v_n = Q_n + iP_n$, $n \in \iota_N$ and J the standard symplectic matrix in $\mathbf{R}^{2N}$. Also for F a C^2 function on $U \subset \mathbf{R}^m$, $x = x_*$ a critical point of F, let $\nabla^2 F(x_*)$ denote the matrix of partial derivatives $\partial_{x_i}\partial_{x_j}F$ at $x = x_*$, i.e. the Hessian in the coordinates x. Then the linearized system can be written as

$$\dot{w} = J\mathcal{H}w, \quad \text{with } \mathcal{H} = \nabla^2 h_\omega(A). \tag{A.2}$$

The dependence of $\mathcal{H}$ on ω, and A is suppressed from the notation. The relative stability of the breather is obtained the spectra of $J\mathcal{H}$, and $\mathcal{H}$; see e.g. [13].

Alternatively, given the fixed point $A \in \mathbf{C}^N$ of (A.1), and assuming $A_k \neq 0$, $\forall k \in \iota_N$, let $a \in S_c^{N-1} \times \mathbf{T}^{N-1}$ denote the corresponding point in the reduced phase space via (2.4), (2.5). Also let $c = P(A)$. Then a is a fixed point of (2.7). The linearization of (2.7) around a is

$$\dot{y} = J_c\overline{\mathcal{H}}y, \quad \text{with } \overline{\mathcal{H}} = \nabla^2 h_c(a), \tag{A.3}$$

where $\overline{\mathcal{H}}$ is the Hessian at a in the $\bar{I}, \bar{\theta}$ system of (2.4), (2.5), $y \in \mathbf{R}^{2(N-1)}$, and J_c is the standard symplectic matrix in $\mathbf{R}^{2(N-1)}$.

The spectra $\sigma(J\mathcal{H})$, $\sigma(J_c\overline{\mathcal{H}})$ are related in a simple way in Proposition A.1 below. To describe the relation between $\sigma(\overline{\mathcal{H}})$, $\sigma(\mathcal{H})$ define the variables $\tilde{I}, \tilde{\theta}$ by $v = f(\tilde{I}, \tilde{\theta})$, i.e. these are the action-angle variables in the moving frame. Let $A = f(\tilde{A})$. Let $\tilde{H}_\omega$ denote H_ω in the variables $\tilde{I}, \tilde{\theta}$, and let $\tilde{h}_\omega = \frac{1}{2}\tilde{H}_\omega$. The linearization of the corresponding Hamiltonian system around the fixed point $\tilde{A}$ is

$$\dot{w} = J\tilde{\mathcal{H}}w, \quad \text{with } \tilde{\mathcal{H}} = \nabla^2\tilde{h}_\omega(\tilde{A}). \tag{A.4}$$

Also define $\beta \in \mathbf{R}^{2N-2}$ by $\beta_{2j-1} = \partial_{I_j}\partial_{I_N}h_\omega(\tilde{A})$, $\beta_{2j} = \partial_{\theta_j}\partial_{I_N}h_\omega(\tilde{A})$, $j = 1, \ldots, N-1$, and let $\gamma = \partial_{I_N}^2 h_\omega(\tilde{A})$. Recall that the *index* of a symmetric matrix M is the dimension of the maximal subspace where M is negative definite.

Proposition A.1. (i) $\sigma(J\mathcal{H}) = \sigma(J_c\overline{\mathcal{H}}) \cup \{0\}$. (ii) *Let* $\sigma(\overline{\mathcal{H}})$ *consist of* $2N - 2$ *eigenvalues* $\lambda_1 \leq \lambda_2 \leq \cdots \leq \lambda_{2N-2}$. *Then* $\tilde{H}$ *has a zero eigenvalue, and* $2N - 1$ *eigenvalues* $\rho_1, \ldots, \rho_{2N-1}$ *that satisfy*

$$\rho_1 \leq \lambda_1 \leq \rho_2 \leq \lambda_2 \leq \cdots \leq \rho_{2N-2} \leq \lambda_{2N-2} \leq \rho_{2N-1}. \tag{A.5}$$

In the case where $\lambda_1 < \lambda_2 < \cdots < \lambda_{2N-2}$, *and* $\beta_j \neq 0$, $\forall j = 1, \ldots, 2N - 2$, *all inequalities in* (A.5) *become strict. Also,* (iii) $index(\mathcal{H}) = index(\tilde{\mathcal{H}}) = index(\overline{\mathcal{H}}) + s$ *with* $s = 0$ *or* 1. *If* $\overline{\mathcal{H}}$ *is invertible, then* $s = 0$, *if* $\gamma \geq \beta^T\overline{\mathcal{H}}^{-1}\beta$, *and* $s = 1$, *if* $\gamma < \beta^T\overline{\mathcal{H}}^{-1}\beta$.

Proof of Proposition A.1. To see (i) it is enough to compare $\sigma(J_c\overline{\mathcal{H}})$ to $\sigma(J\tilde{\mathcal{H}})$ since $J\mathcal{H}$ and $J\tilde{\mathcal{H}}$ are similar. Let $x_{2j-1} = I_j$, $x_{2j} = \theta_j$, $j \in \iota_N$, $F_j = (-1)^j\partial_{x_j}\tilde{h}_\omega$, $j \in \iota_N$, and $\tilde{M}_{i,j} = \partial_{x_j}F_i$ evaluated at $\tilde{A}$, $i, j \in \iota_{2N}$, i.e. $\tilde{M}$ is $J\tilde{\mathcal{H}}$ with its entries renumbered. Similarly, let $\bar{I}_j = I_j$, $\bar{\theta}_j = \theta_j$, $j \in \iota_{N-1}$, $y_{2j-1} = \bar{I}_j$, $y_{2j} = \bar{\theta}_j$, $j \in \iota_{N-1}$, $f_j = (-1)^j\partial_{y_j}h_c$, $j \in \iota_N$, and let $\overline{M}_{i,j}$ be $\partial_{y_j}f_i$ evaluated at $a = y(A)$, $i, j \in \iota 2N$, i.e. $\overline{M}$ is $J_c\overline{\mathcal{H}}$ with its entries renumbered. Then

$$\tilde{M}_{i,j} = \frac{\partial F_i}{\partial x_j}(a) = (-1)^i \frac{\partial^2 h_\omega}{\partial x_i\partial x_j}(x)|_{x=A}$$

$$= (-1)^i \frac{\partial^2 h_\omega}{\partial y_i\partial y_j}(y, J_n)|_{y=a, J_N=Nc}. \tag{A.6}$$

By the continuity of the partial derivatives of H_ω, and the definitions of h_ω, h_c we then have

$$\tilde{M}_{i,j} = (-1)^i \frac{\partial^2 h_\omega}{\partial y_i\partial y_j}(y, Nc)|_{y=a} = (-1)^i \frac{\partial^2 h_\omega}{\partial y_i\partial y_j}(y, Nc)|_{y=a}$$

$$= (-1)^i \frac{\partial^2 h_c}{\partial y_i\partial y_j}(y)|_{y=a} = \overline{M}_{i,j}. \tag{A.7}$$

Therefore

$$\tilde{M}_{i,j} = \overline{M}_{i,j}, \quad \forall i, j \in \iota_{N-1}. \tag{A.8}$$

Furthermore,

$$\frac{\partial F_j}{\partial\theta_N} = (-1)^j \frac{\partial^2 H_\omega}{\partial x_j\partial\theta_N} \equiv 0, \qquad \frac{\partial F_{2N-1}}{\partial x_j} = (-1)^j \frac{\partial^2 H_\omega}{\partial x_j\partial\theta_N} \equiv 0,$$

$$\forall j \in \iota_N, \tag{A.9}$$

therefore

$$\tilde{M}_{j,2N} = \tilde{M}_{2N-1,j} = 0, \quad \forall j \in \iota_N. \tag{A.10}$$

Combining (A.8), (A.10) we then have

$$\det(M - \lambda\mathit{l}_{2N}) = \lambda^2 \det(\tilde{M} - \lambda\mathit{l}_{2(N-1)}), \tag{A.11}$$

where l_k is the identity matrix in $\mathbf{R}^k$. (A.11) then immediately implies (i).

To see (ii) we index the entries of each Hessian as above, i.e. $\tilde{\mathcal{H}}_{i,j} = \partial_{x_i}\partial_{x_j}\tilde{h}_\omega$ at $\tilde{A}$, $\overline{\mathcal{H}}_{i,j} = \partial_{y_i}\partial_{y_j}h_c$ at a. Since $\tilde{h}_\omega$ is independent of θ_N the $2N$-th column and row of $\tilde{\mathcal{H}}$ both vanish identically and therefore $\tilde{\mathcal{H}}$ has a zero eigenvalue. To see the remaining eigenvalues define the $(2N - 1) \times (2N - 1)$ matrix R by $R_{i,j} = \tilde{\mathcal{H}}_{i,j}$, $i, j \in \iota_{2N-1}$. Arguing as in (A.6) we have

$$R_{i,j} = \tilde{\mathcal{H}}_{i,j} = \overline{\mathcal{H}}_{i,j}, \quad \forall i, j = \iota_{2N-2}. \tag{A.12}$$

Then (A.5) follows immediately from Cauchy's interlacing eigenvalues theorem for symmetric matrices and their submatrices; see [25, Chapter III.1].

To obtain (A.5) with strict inequalities, note that $R_{i,2N-1} = \beta_i$, $i \in \iota_{2N-1}$, and $R_{2N-1,2N-1} = \gamma$. Let S be an orthogonal matrix S satisfying $S\overline{\mathcal{H}}S^{-1} = \Lambda$, where Λ is diagonal, with $\Lambda_{j,j} = \lambda_j$, $j \in \iota_{2N-2}$. Then R is similar to

$$\tilde{R} = \begin{bmatrix} S\overline{\mathcal{H}}S^{-1} & S\beta \\ \beta^TS^{-1} & \gamma \end{bmatrix} = \begin{bmatrix} \Lambda & \tilde{\beta} \\ \tilde{\beta}^T & \gamma \end{bmatrix} \tag{A.13}$$

where $\tilde{\beta} = S\beta$. We see by induction that

$$\det(\tilde{R} - \rho\mathit{l}_{2N-1}) = (\gamma - \rho)\prod_{j\in\iota_{2N-2}}(\lambda_j - \rho)$$

$$- \sum_{k\in\iota_{2N-2}}\tilde{\beta}_k^2\prod_{j\in\iota_{2N-2}\setminus\{k\}}(\lambda_j - \rho). \tag{A.14}$$

Let $G(\rho) = \det(\tilde{R} - \rho\mathit{l}_{2N-1})$. Clearly, the roots of G are eigenvalues of $\tilde{\mathcal{H}}$. By (A.14), and the assumptions on the λ_j and $\tilde{\beta}_k$, we have that $G(\lambda_k) \neq 0$ and has sign $(-1)^k$, $\forall k \in \iota_{2N-1}$. Thus G has at least one root between every pair of consecutive λ_j. By (A.14) the highest degree term of the polynomial G is $-\rho^{2N-1}$, therefore

$\lim_{\rho \to \pm\infty} G(\rho) = \mp\infty$. Since $G(\lambda_1) < 0$, and $G(\lambda_{2N-2}) > 0$, G has at least two roots $\rho_1 < \lambda_1$, and $\rho_{2N-1} > \lambda_{2N-2}$. Since G can have at most $2N - 1$ roots, we have $\rho_1 < \lambda_1 < \rho_2 < \lambda_2 < \cdots < \rho_{2N-2} < \lambda_{2N-2} < \rho_{2N-1}$.

For (iii) we note that (A.5) implies index$(\tilde{\mathcal{H}})$ = index$(\overline{\mathcal{H}}) + s$ with $s = 0$ or 1. On the other hand $\tilde{\mathcal{H}}$, $\mathcal{H}$ are the Hessians at a critical point in different coordinates and have the same index. Also, index$(\tilde{\mathcal{H}})$ = index(R), and if $\overline{\mathcal{H}}$ is invertible, then det$(R) = (\gamma - \beta^T \overline{\mathcal{H}}^{-1} \beta)$ det$(\overline{\mathcal{H}})$, see e.g. [26, p. 144], or

$$(-1)^r \prod_{j=1}^{2N-1} |\rho_j| = (\gamma - \beta^T \overline{\mathcal{H}}^{-1} \beta)(-1)^{\overline{h}} \prod_{j=1}^{2N-2} |\lambda_j|, \qquad (A.15)$$

where $r = $ index(R), $\overline{h} = $ index$(\overline{\mathcal{H}})$. For $\gamma \neq \beta^T \overline{\mathcal{H}}^{-1} \beta$ the statement follows from the fact that $s = 0$, or 1. The case $\gamma = \beta^T \overline{\mathcal{H}}^{-1} \beta$ follows from (A.5) and (A.15). $\square$

References

[1] D.N. Christodoulides, R.I. Joseph, Discrete self-focusing in nonlinear arrays of coupled waveguides, Opt. Lett. 18 (1988) 794.
[2] D.N. Christodoulides, F. Lederer, Y. Silberberg, Discretizing light behavior in linear and nonlinear lattices, Nature 424 (2003) 817–823.
[3] G.L. Alfimov, P.G. Kevrekidis, V.V. Konotop, M. Salerno, Wannier function analysis of the nonlinear Schrödinger equation with a periodic potential, Phys. Rev. E 66 (2002) 46608.
[4] J.C. Eilbeck, P.S. Lomdahl, A.C. Scott, The discrete self-trapping equation, Physica D 16 (1985) 318–338.
[5] C. Antonopoulos, T. Bountis, C. Skokos, Chaotic dynamics of N-degree of freedom Hamiltonian systems, Int. J. Bifurc. Chaos 16 (2006) 1777–1793.
[6] R. Abraham, J. Marsden, Foundations of Mechanics, W.A. Benjamin, Reading, 1978.
[7] P. Panayotaros, Continuation of breathers in a finite discrete NLS equation, Disc. Cont. Dyn. Syst. S 4 (5) (2011) 1227–1245.
[8] Yu.V. Bludov, V.V. Konotop, Surface modes and breathers in finite arrays of nonlinear waveguides, Phys. Rev. E 76 (2007) 046604.
[9] T. Kapitula, P.G. Kevrekidis, Z. Chen, Three is a crowd: solitary waves in photorefractive media with three potential wells, SIAM J. Appl. Dyn. Syst. 5 (2007) 598–633.
[10] P. Panayotaros, Continuation of normal modes in finite NLS lattices, Phys. Lett. A 374 (38) (2010) 3912–3919.
[11] E. Canalias, A. Delshams, J.J. Masdemont, P. Roldan, The scattering map in the planar three body problem, Celestial Mech. Appl. 95 (2006) 155–171.
[12] J. Milnor, Morse Theory, Princeton Univ. Press, Princeton, 1973.
[13] D.E. Pelinovsky, P.G. Kevrekidis, D.J. Frantzeskakis, Stability of discrete solitons in nolinear Schrödinger lattices, Physica D 212 (2005) 1–19.
[14] S. Smale, Topology and Mechanics I: Invent. Math. 10 (1970) 305–331.
[15] R.S. MacKay, S. Aubry, Proof of existence of breathers for time-reversible or Hamiltonian networks of weakly coupled oscillators, Nonlinearity 7 (1994) 1623–1643.
[16] P. Panayotaros, Linear stability of real breathers in the discrete NLS, Phys. Lett. A 373 (2009) 957–963.
[17] Y.S. Kivshar, D.K. Cambell, Peirls–Nabarro barrier for highly localized nonlinear modes, Phys. Rev. E 48 (1993) 3077–3081.
[18] M. Öster, M. Johansson, A. Eriksson, Enhanced mobility of strongly localized modes in waveguide arrays by inversion of stability, Phys. Rev. E 67 (2003) 056606.
[19] C. Robinson, Dynamical Systems: Stability, Symbolic Dynamics, and Chaos, CRC Press, Boca Raton, 1995.
[20] K.R. Meyer, G.R. Hall, Introduction to Hamiltonian Dynamical Systems and The N-Body Problem, Springer, New York, 1992.
[21] M.J.D. Powell, A hybrid method for nonlinear equations, in: P. Rabinowitz (Ed.), Numerical Methods for Nonlinear Algebraic Equations, Gordon and Breach, New York, 1970.
[22] A.J. Homburg, B. Sandstede, in: H.W. Broer, B. Hasselblatt, F. Takens (Eds.), Homoclinic and Heteroclinic Bifurcations of Vector Fields, in: Handbook of Dynamical Systems, vol. 3, Elsevier, Amsterdam, 2010.
[23] O. Bang, P.D. Miller, Exploiting discreteness for switching in arrays of nonlinear waveguides, Phys. Scripta T67 (1996) 26–29.
[24] S. Aubry, T. Cretegny, Mobility and reactivity of discrete breathers, Physica D 119 (1998) 34–46.
[25] R. Bhatia, Matrix Analysis, Springer, New York, 1997.
[26] D.S. Bernstein, Matrix Mathematics: Theory, Facts, and Formulas with Application to Linear Systems Theory, Princeton Univ. Press, Princeton, 2005.